Eur. J. Mineral.
PrePub DOI: 10.1127/ejm/2015/0027-2492

PrePub Article
Special issue dedicated to Thomas Armbruster

The modular structure of pyroxenes

MASSIMO NESPOLO[1,*] and MOIS I. AROYO[2]

[1] Department of Geology and Mineralogy, Faculty of Science, Kyoto University, Kitashirakawaoiwake-cho, Sakyo-ku, Kyoto-shi 606–8502, Japan
*Corresponding author, e-mail: massimo.nespolo@crm2.uhp-nancy.fr
[2] Física de la Materia Condensada, Facultad de Ciencia y Tecnología, Universidad del País Vasco, Apartado 644, 48080 Bilbao, Spain

Abstract: The structures of pyroxenes can be described as cell-twins based on a common module (a layer) consisting of half the unit cell of the $P2_1/c$ polymorph. Atomic models of the different polymorphs are computed and the close similarity between the models and the corresponding experimental structures is shown. The cell-twin operations building the structures of pyroxenes are partial operations belonging to a special case of space groupoid which was called ''twinned space group'' in the pioneering studies by Ito started in 1935. The groupoid analysis of clino-, proto- and orthoenstatite is presented and the special place occupied by pyroxenes in the category of polytypes is discussed.

Key-words: cell-twinning; enstatite; local symmetry; partial symmetry; polytypism; pyroxenes; space groupoids; twinned space groups.

1. Introduction

Warren & Modell (1930) first reported the structure of enstatite and pointed out its relation with that of diopside: the former can be roughly obtained from the latter by a glide reflection perpendicular to the orthorhombic **a** axis, disregarding the chemical differences in the M2 site. Ito (1935) took the opposite view, starting from the diopside structure described in a pseudo-orthorhombic cell, and showed that the systematic absences in this cell are compatible with the polysynthetic repetition of the diopside structure through a *b*-glide perpendicular to the **a** axis of the pseudo-orthorhombic cell. This observation led him to adopt a more general description of the symmetry of the pyroxene structures based on an extension of the group structure obtained by superposing to the space group a set of operations reminiscent of the twin operations mapping domains or individuals in a twinned crystal. Based on this analogy, he called the set of operations a ''twinning group'' and the result of the extension of the space group a ''twinned space group'' (Ito, 1938). According to Ito's definition, the operations of the ''twinning group'' act on a domain corresponding to ''a multiple (or submultiple) of that of the original unit cell'', so that a ''new cell is formed, governed by the operation of the twinning group'' (Ito, 1950).

According to modern usage, the polysynthetic structures, as later termed by Sadanaga (1978), which were the object of Ito's investigation, are *monoarchetypal modular structures* (Makovicky, 1997; Ferraris *et al*., 2008), *i.e*. structures built by periodically juxtaposing one module. The module is a three-dimensional but less than triperiodic object which can ideally be described as cut from a (real or hypothetical) structurally and chemically homogeneous parent structure: the *archetype*. In the above example, making abstraction from the Ca *vs*. Mg difference in the M2 site and allowing some small deviation in the atomic coordinates, the diopside is the archetype, while the enstatite is a structure derived from it. The operations relating the modules are *cell-twinning operations* and monoarchetypal structures are also known as cell-twins (Nespolo *et al*., 2004). The operations that Ito collected in the ''twinning group'' are partial operations which, together with the total operations of the space group, form a groupoid in the sense of Brandt (1927) (for details, see Ito & Sadanaga, 1976; Sadanaga, 1978). A groupoid analysis has been presented by the OD school (Sedlacek *et al*., 1979) but using two modules whose relation with the modular nature of pyroxenes is less immediate: we present here an alternative analysis which uses directly the module which can be seen as a common denominator of all the pyroxenes.

Ohashi (1984) analysed the polysynthetic relation between clino- and orthoenstatite and completed Ito's interpretation by adding the cell-twin operations that are

Massimo NESPOLO: On leave from Université de Lorraine, Faculté des Sciences et Technologies, Institut Jean Barriol, FR 2843, CRM2 UMR - CNRS 7036.

DOI: 10.1127/ejm/2015/0027-2492
0935-1221/15/0027-2492 $ 6.75

equivalent under the space group of the crystal. This would correspond to decomposing the space groupoid in cosets with respect to the space group, but no groupoid analysis was given in Ohashi's description. Meanwhile, Brown *et al*. (1961) had suggested a more general structural relation, extending to protoenstatite as well, based on the displacement of the SiO_3 chains of either $+c/3$ (+) or $-c/3$ (−) along the **a** axis of the clino-enstatite, so that the three polymorphs would correspond to the sequence ++++ (clino), + − + − (proto) and ++− (ortho), when expressed in a unit cell with comparable *a* parameter.

The above set of observations has prompted us to challenge a unifying modular interpretation of the pyroxene structures where the full relations among the atomic positions in the various polymorphs can be obtained once the module is correctly identified. The purpose of a modular description of crystal structures is to point out the existence of one or more common building blocks as well as the operations relating these blocks in the various structures of the series. The module(s) building one polymorph is(are) conserved, apart from secondary effects like the thermal expansion, while the relative position and/or orientation of successive modules are modified. As we are going to see, this is what happens in pyroxenes and the results show a very close similarity between the structures of the three polymorphs based on the cell-twinned model of clinoenstatite. The estimation of the structural similarity between the cell-twinned clinoenstatite and the orthorhombic polymorphs is obtained with the COMPSTRU routine at the Bilbao Crystallographic Server (see Tasci *et al*., 2012, and Aroyo *et al*., 2006 respectively) and the results are expressed by four parameters:

- the *degree of lattice distortion* is the spontaneous strain (the square root of the sum of squared eigenvalues of the strain tensor divided by 3);
- the *maximum distance* shows the maximal displacement between the atomic positions of the paired atoms;
- the *arithmetic mean*, $d_{av} = \sum_i m_i u_i / n$, where m_i is the multiplicity of the Wyckoff position in the primitive unit cell, u_i is the atomic displacement of the *i*-th atomic position and *n* is the number of atoms in the primitive unit cell;
- the *measure of similarity* is a function of the differences in atomic positions (weighted by the multiplicities of the sites) and the ratios of the corresponding lattice parameters of the structures (Bergerhoff *et al*., 1999).

2. Structure, composition and polymorphism of pyroxenes

The structure of pyroxenes is well known, we give here a very brief summary to remind some features of use in the following discussion (for details, see Cameron & Papike, 1981).

Figure 1 shows a schematic structure of pyroxenes seen in projection along the **a** (left) and **c** (right) axes. Chains of corner-sharing tetrahedra with apical and basal oxygen atoms produce respectively octahedral sites (M1) and larger, less well-defined sites (M2) occupied by a variety of cations. The tetrahedral chains are drawn in different colours because in some pyroxenes (those crystallising in space-group types *Pbca*, $P2_1/c$ and $P2/n$) they are crystallographically independent (unrelated by symmetry operations of the space group).[1] The oxygen atom forming a bridge between two tetrahedra in a chain, commonly known as the O3 oxygen, is the flexible point of the pyroxene structure: rotations

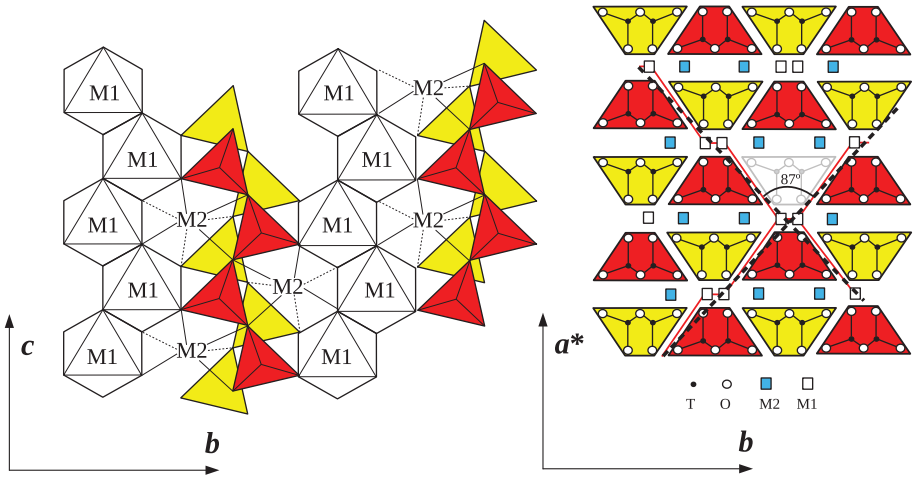

Fig. 1. Schematic view of the pyroxenes structure in projection along the **a** (left) and **c** (right) axes. The tetrahedral chains are drawn in different colours to emphasize their crystallographic independence in some of the space-group types in which pyroxenes crystallise (*Pbca*, $P2_1/c$ and $P2/n$). In the right part of the figure the **a*** axis is indicated to make it valid for both ortho- and clinopyroxenes. The red full lines indicate the regions of weaker bonds, which correspond to the 87° macroscopic cleavage, shown by black dashed lines (modified after Nespolo *et al*., 1999). (online version in colour)

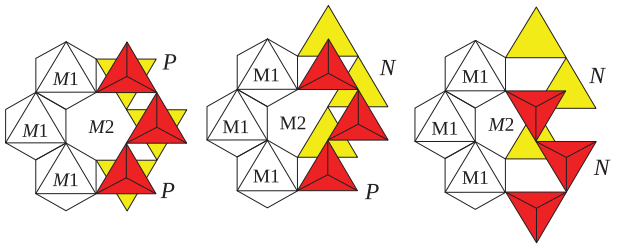

Fig. 2. The size of the M2 site decreases for tetrahedral chain configuration moving from PP (*C*2/*c* pyroxenes with the exception of spodumene; omphacites, augites), to PN (orthopyroxenes, low-clinoenstatite) to NN (protopyroxenes, spodumene) configuration. The chains are shown in their extreme configuration, corresponding to a 120° O3-O3-O3 angle, but this is hardly realized in any experimental condition, the actual angle depending on the conditions and being intermediate between 120° and 180° (modified after Cameron & Papike, 1981). (online version in colour)

about this oxygen allow the structure to respond to the variations in the external conditions (temperature, pressure) and to adapt to the presence of cations of different size.

Figure 2 emphasizes the effect of the relative rotations of the tetrahedral chains on the size of the M2 site, which decreases from PP to PN to NN configuration (P for positive, N for negative, meaning the same or opposite orientation of the triangular bases of the tetrahedra with respect to the triangular faces of the octahedra with which the chains share one of their basal oxygen atoms). The chains are shown in their extreme configuration, corresponding to a 120°O3-O3-O3 angle, which is hardly realized in any experimental conditions; depending on the experimental conditions the angle varies between 120° and 180°.

The general formula of pyroxenes, $^{[6-8]}X^{[6]}Y^{[4]}Z_2O_6$, allows for a wide range of compositions. The digit in square brackets gives the coordination number; X represents the cations entering in the M2 site, whose coordination number depends on the P or N rotations of the tetrahedral chains and on the O3-O3-O3 angle, Y are the cations occupying the M1 site, and Z are the cations in the tetrahedra. Accordingly, a general composition scheme for most of the naturally occurring pyroxenes can be represented as follows (Morimoto *et al*., 1988):

- ferromagnesian pyroxenes, $X = Y = (Mg_wFe_{1-w})_{0.95-1}Ca_{0-0.05}$, $Z = Si$; end-members are enstatite ($w = 1$) and ferrosilite ($w = 0$);
- calcic pyroxenes, X = Ca; end-members are diopside (Y = Mg, Z = Si), hedenbergite ($Y = Fe^{2+}$, Z = Si), johannsenite ($Y = Mn^{2+}$, Z = Si), petedunnite (Y = Zn, Z = Si), esseneite ($Y = Fe^{3+}$, Z = Al,Si);
- pyroxenes of intermediate composition: $X = Ca_w(Mg,Fe)_{1-w}$, Y = (Mg,Fe): pigeonites ($0.05 \leq w \leq 0.2$), augites ($0.2 \leq w \leq 0.45$);
- sodic pyroxenes, $NaMFeSi_2O_6$, M = Al (jadeite), Fe (aegirine), Cr (kosmochlor), Sc (jervisite);
- lithium-pyroxenes: spodumene, $LiAlSi_2O_6$.

A wide range of solid solutions exist among several of the end-members, and the same term is often used to indicate both the end-member and a composition range including it. For example, the term ''enstatite'' can be used to indicate the pure end-member $Mg_2Si_2O_6$ or the compositional field defined by $Mg_2Si_2O_6$, $Mg_{1.95}Ca_{0.05}Si_2O_6$, $MgFeSi_2O_6$ and $Mg_{0.975}Fe_{0.975}Ca_{0.05}Si_2O_6$. Similarly, jadeite can indicate, besides the end-member, the composition field $(Na_xCa_{1-x})(Al_yFe_{1-y})Si_2O_6$ with $0 \leq x \leq 0.2$ and $0 \leq y \leq 0.5$, and aegirine the composition field corresponding to the same formula but with $0.5 \leq y \leq 1$. For $0.2 \leq x \leq 0.8$ the terms omphacite and aegirine-augite are used for $0 \leq y \leq 0.5$ and $0.5 \leq y \leq 1$ respectively. Unless specified otherwise, when a term can indicate an end-member or a solid solution, in the following we make reference to the former.

We are interested in the structure relations among the various pyroxenes; therefore we largely make abstraction from the chemical composition but rather consider the spatial position of atoms with the same type of coordination. The chemical nature of those atoms leads to small differences in the cell parameters and fractional coordinates but this has no influence on the structural relations, which correspond to polymorphism when the chemistry is the same. For example, (ortho)enstatite and clinoenstatite are clearly polymorphs when they have the same composition, but not when they represent different points in the composition range of enstatite. In the following we implicitly assume the same composition when speaking of polymorphism.

Pyroxenes occur in various space-group types:

- *Pbca*, for orthorhombic pyroxenes (enstatite and ferrosilite with calcium content lower than 0.05 per formula unit);
- *Pbcn*, or ''protopyroxenes'', occurring for the composition of enstatite or very close to it;
- $P2_1cn$, reported in a series of high-pressure experiments on $(Mg_{1.54}Li_{0.23}Sc_{0.23})Si_2O_6$ with protopyroxene structure (Yang *et al*., 1999);
- $P2_1/c$, for clinopyroxenes in the compositional field of enstatite–ferrosilite and of pigeonites (low-temperature);
- *C*2/*c*, for clinopyroxenes in the compositional field of augites, omphacites (high-temperature), pigeonites (high-temperature), sodic-pyroxenes, spodumene, as well as high-temperature phase of enstatite–ferrosilite;
- *P*2/*n*, in the compositional field of omphacites (low-temperature).

The tetrahedral chains have configuration PP in augites, high-temperature clinopyroxenes; PN in orthopyroxenes and low-temperature clinopyroxenes; NN in protopyroxenes and spodumene (Griffen, 1992). The NN configuration corresponds to the smallest M2 site and is realized for small cations, like lithium in spodumene and magnesium in proto-enstatite. The latter however exists only at high

temperature and low pressure, conditions favouring an increase in the size of the M2 site due to thermal expansion.

Because enstatite occurs in all the space-group types mentioned above but $P2/n$, in the following we take it as representative and analyse the structure of the enstatite (pure end-member Mg_2SiO_6) polymorphs. The structures of the other pyroxenes are then obtained by replacing the atoms in enstatite by different species, allowing small relaxations which take into account the difference in the atomic dimensions. Concretely, we will use the following terminology, widely present in the literature, although not all these terms correspond to accepted mineral names.

- *high-clinoenstatite*, space-group type $C2/c$; it occurs in two variants, one at high-pressure, unquenchable, and the other at high-temperature, quenchable, the two being possibly related by a first-order phase transition (Shimobayashi *et al*., 1998); the crystal structure of the high-temperature high-clinoenstatite was reported by Yoshiasa *et al*. (2013), with cell parameters $a = 9.5387$ Å, $b = 8.6601$ Å, $c = 5.2620$ Å, $\beta = 108.71°$; the high-pressure phase is unquenchable, but the corresponding phase in ferrosilite is stable: we use its coordinates (Hugh-Jones *et al*., 1994) and confirm the close similarity of the two structures;
- *low-clinoenstatite*, stable at ambient conditions, crystallizing in a space group of type $P2_1/c$; the crystal structure was reported more than once, here we make reference to Ohashi (1984), who reported cell parameters $a = 9.606$ Å, $b = 8.8131$ Å, $c = 5.170$ Å, $\beta = 108.35°$.
- *orthoenstatite*, stable at ambient conditions, crystallizing in a space group of type *Pbca*; here we make reference again to Ohashi (1984), who reported cell parameters $a = 18.225$ Å, $b = 8.8128$ Å, $c = 5.180$ Å;
- *protoenstatite*, stable at high temperature and low pressure, not quenchable, crystallizing in a space group of type *Pbcn*; here we make reference to the structure reported by Yang & Ghose (1995) in a high-temperature (1360 K) experiment, who found cell parameters $a = 9.306$ Å, $b = 8.886$ Å, $c = 5.360$ Å.

The $P2_1cn$ structure reported by Yang *et al*. (1999) is simply a distortion of the protopyroxene structure; each of the Si and O atomic positions in *Pbcn* are split into pairs obtained by the inversion lost in the phase transition followed by a small relaxation (maximal deviation for the O3 oxygen atom, which is the bridge between two tetrahedra in a chain). The structure is thus still pseudo-symmetric with respect to the parent phase and does not need to be considered separately.

In the official nomenclature of pyroxenes (Morimoto *et al*., 1988) the two orthorhombic polymorphs are differentiated as enstatite-*Pbca* and enstatite-*Pbcn*, respectively. However, the terms used widely in the literature are orthoenstatite and protoenstatite. In the same way, the two monoclinic polymorphs are not listed under separate mineral names, yet the terms ''high-'' and ''low-'' clinoenstatite are widespread in the literature. In the following, in the need to clearly differentiate these four polymorphs of enstatite, we stick to their names widely used in the literature.

The relation between the cell parameters of the clino- and orthoenstatite was given by Ito (1935): $\mathbf{a}_{ortho} = 2\mathbf{a}_{clino} - \mathbf{c}_{clino}$, $\mathbf{b}$ and $\mathbf{c}$ being in common. This applied to the axial setting chosen by Warren & Modell (1930), with acute monoclinic angle. Modern reports give an obtuse angle so that the transformation becomes $\mathbf{a}_{ortho} = 2\mathbf{a}_{clino} + \mathbf{c}_{clino}$ (Sadanaga *et al*., 1969). If we apply this transformation to the low-clinoenstatite cell parameters given above, we obtain $a = 18.2562$ Å, $b = 8.8131$ Å, $c = 5.170$ Å, $\beta = 92.76°$, which are close to the cell parameters of the orthoenstatite. To be noted that the β angle deviates slightly from 90° so that the above transformation leads to a pseudo-orthorhombic cell.

The high and low clinoenstatite show a group-subgroup relation and are related by a displacive phase transition. The space group of the low-clinoenstatite is a klassengleiche subgroup of that of the high-clinoenstatite: the geometric crystal class is the same, but half of the symmetry operations are lost in the transition (all those generated by the C centring translation). Consequently, in this phase transition antiphase domains but no twin domains could arise. Antiphase domain boundaries have indeed been observed by electron microscopy following the $C2/c$ to $P2_1/c$ transition from high- to low-pigeonite, which is isostructural to enstatite (Shimobayashi, 1992). The phase transition from protoenstatite to low-clinoenstatite is of martensitic type (Smyth, 1974; Boysen *et al*., 1991) and allow twins but not antiphase domains. No direct phase transition is observed between ortho- and low-clino enstatite, both being the product of transition from protoenstatite, favoured by the absence (ortho) or presence (clino) of shear stress, respectively (Smyth, 1974). The corresponding space-group types, *Pbca* and $P2_1/c$, are not in group-subgroup relation. *Pbcn* and *Pbca* are not in a group-subgroup relation either but the corresponding phases (proto- and orthoenstatite) are related by a phase transition. A structural relation between proto- and orthoenstatite can be found only through an intermediate common subgroup or supergroup: the transformation is much more sluggish than the proto- to clino and the high-clino to low-clino transitions and needs slow cooling rates to produce ordered orthoenstatite from protoenstatite (Boysen *et al*., 1991), which is indicative of a reconstructive phase transition.

In general, the same scheme of phase transitions holds for ferrosilite, the iron-counterpart of enstatite, with the difference that at low pressure the pyroxene structure is unstable and decomposes in olivine and quartz (Lindsley, 1980).

3. The fundamental pyroxene module

First of all, we note (Table 1) that the structure of low-clinoenstatite reported by Ohashi (1984) in $P2_1/c$ is pseudosymmetric with respect to $C2/c$ (axial settings related by an origin shift $\frac{1}{4}\frac{1}{4}0$). The atomic displacements necessary to acquire the higher space-group symmetry vary from 0.1706 Å for Mg to 0.5599 Å for two of the six oxygen atoms (the pseudo-symmetry analysis is performed with the PSEUDO routine at the Bilbao Crystallographic Server: Capillas *et al*., 2011). The low-clinoenstatite structure idealized to $C2/c$ symmetry is very close to the high-clinoenstatite structure experimentally determined by Yoshiasa *et al*. (2013; with respect to the published coordinates, we use the equivalent description obtained by shifting the origin $\frac{1}{2}$ along **a**, which is one of the operations in the Euclidean normalizer of $C2/c$[2]).

In the following we use the idealized structure of the low-clinoenstatite in the $P2_1/c$ setting: unless specified otherwise, this is the structural model we refer to when saying simply ''clinoenstatite''. Half of this structure is the fundamental pyroxene module; the operations repeating this module according to the clino-, proto- and ortho enstatite topology give the idealized structures of the corresponding polymorphs; the real structures are then seen as a desymmetrization (relaxation) of the structures obtained in this way.

Table 2 shows the fractional atomic coordinates in the whole unit cell of clinoenstatite in the $P2_1/c$ axial setting. Atoms are arranged so that those in first module occupy the first four columns and those in the second module are in the second four columns and are obtained from the previous ones by the transformation $x,y,z \rightarrow x + \frac{1}{2},y + \frac{1}{2},z$. The structure can thus be ideally divided into two modules having their boundary at $x = \frac{1}{2}$. The operation mapping a module onto the next one is a translation by half of the *a* parameter of the unit cell (a full module translation along **a**) and a half-translation along **b**, with no change along **c** Fig. 3. This module corresponds to what Ito (1950) called ''a submultiple of the original unit cell''. Given the monoclinic angle of about 108°, the mapping of two adjacent modules corresponds to a constant stacking of the module along **a**, in agreement with the ++ sequence given by Brown *et al*. (1961).

Either of the two modules with *x* coordinate in the two intervals *a*/2 apart can be taken as fundamental module. We choose the one with *x* coordinate between $\frac{1}{2}$ and 1, which correspond to the *x* coordinate between $\frac{1}{4}$ and $\frac{1}{2}$ in the cell of orthoenstatite used by Ohashi (1984). In the following, we use this module to build up the model structures of the other polymorphs: the comparison with the experimental coordinates will show how close these models are to the real structures.

Table 1. Atomic coordinates of low-clinoenstatite taken from Ohashi (1984) (structure in $P2_1/c$), idealized to the $C2/c$ supergroup of high-clinoenstatite but still described in the subgroup (idealized structure in the setting of $P2_1/c$) and the corresponding description in the supergroup (idealized structure in the setting of $C2/c$). The atomic coordinates in the HT high-clinoenstatite show a close similarity with those of the idealized low-clinoenstatite (pairs of oxygen orbits in $P2_1/c$ coalesce to single orbits in $C2/c$). An origin shift of $\frac{1}{4}\frac{1}{4}0$ relates the settings of $P2_1/c$ and of $C2/c$. The HP high-clinoenstatite being unquenchable, the structure of the high-clinoferrosilite, a stable phase occurring in the phase diagram of ferrosilite, is used instead.

Structure in $P2_1/c$					Idealized structure in the setting of $P2_1/c$			
Atomic site	Wyckoff position	*x*	*y*	*z*	*x*	*y*	*z*	Displacement (Å)
Mg 1	4*e*	0.25111	0.65330	0.21770	$\frac{1}{4}$	0.65330	$\frac{1}{4}$	0.1706
Mg 2	4*e*	0.25581	0.01312	0.21460	$\frac{1}{4}$	0.01312	$\frac{1}{4}$	0.2075
Si A	4*e*	0.04331	0.34088	0.29449	0.04835	0.33903	0.26228	0.1882
Si B	4*e*	0.55339	0.83718	0.23007	0.54835	0.83903	0.26228	0.1882
O 1A	4*e*	0.86670	0.33960	0.18510	0.87145	0.33975	0.15490	0.1759
O 1B	4*e*	0.37620	0.83990	0.12470	0.37145	0.83975	0.15490	0.1759
O 2A	4*e*	0.12280	0.50090	0.32180	0.12840	0.49170	0.35545	0.1840
O 2B	4*e*	0.63400	0.98250	0.38910	0.62840	0.99170	0.35545	0.1840
O 3A	4*e*	0.10660	0.27950	0.61530	0.10595	0.23685	0.53465	0.5599
O 3B	4*e*	0.60530	0.69420	0.45400	0.60595	0.73685	0.53465	0.5599

Idealized structure in the setting of $C2/c$					High-clinoenstatite (Yoshiasa *et al*., 2013)			High-ferrosilite (Hugh-Jones *et al*., 1994)		
Atomic site	Wyckoff position	*x*	*y*	*z*	*x*	*y*	*z*	*x*	*y*	*z*
Mg 1	4*e*	$\frac{1}{2}$	0.90330	$\frac{1}{4}$	$\frac{1}{2}$	0.90420	$\frac{1}{4}$	$\frac{1}{2}$	0.90540	$\frac{1}{4}$
Mg 2	4*e*	$\frac{1}{2}$	0.26312	$\frac{1}{4}$	$\frac{1}{2}$	0.28560	$\frac{1}{4}$	$\frac{1}{2}$	0.27121	$\frac{1}{4}$
Si	8*f*	0.29835	0.58903	0.26228	0.29223	0.59198	0.2457	0.2988	0.5882	0.2225
O 1	8*f*	0.12145	0.58975	0.15490	0.1130	0.5828	0.1380	0.126	0.595	0.154
O 2	8*f*	0.37840	0.74170	0.35545	0.3636	0.7577	0.3179	0.377	0.733	0.373
O 3	8*f*	0.35595	0.48685	0.53465	0.3543	0.4935	0.5280	0.352	0.553	0.934

Table 2. Fractional coordinates of the idealized clinoenstatite structure in the whole monoclinic unit cell, $P2_1/c$ setting. The structure of clinoenstatite can be ideally divided into two modules having their boundary at $x = 1/2$: atoms with $x < 1/2$ have their corresponding atoms in the second module related by the transformation $x,y,z \rightarrow x + 1/2, y + 1/2, z$.

Mg2,Mg1	x	1/4	1/4	1/4	1/4	3/4	3/4	3/4	3/4
	y	0.01312	0.6533	0.48688	0.8467	0.51312	0.1533	0.98688	0.3467
	z	1/4	1/4	3/4	3/4	1/4	1/4	3/4	3/4
Si1,Si2	x	0.04835	0.04835	0.45165	0.45165	0.54835	0.54835	0.95165	0.95165
	y	0.33903	0.16097	0.16097	0.33903	0.83903	0.66097	0.66097	0.83903
	z	0.26228	0.76228	0.73772	0.23772	0.26228	0.76228	0.73772	0.23772
O3,O2	x	0.10595	0.10595	0.1284	0.1284	0.60595	0.60595	0.6284	0.6284
	y	0.23685	0.26315	0.0083	0.4917	0.73685	0.76315	0.5083	0.9917
	z	0.53465	0.03465	0.85545	0.35545	0.53465	0.03465	0.85545	0.35545
O1,O4	x	0.12855	0.12855	0.37145	0.37145	0.62855	0.62855	0.87145	0.87145
	y	0.66025	0.83975	0.83975	0.66025	0.16025	0.33975	0.33975	0.16025
	z	0.8451	0.3451	0.1549	0.6549	0.8451	0.3451	0.1549	0.6549
O5,O6	x	0.3716	0.3716	0.39405	0.39405	0.8716	0.8716	0.89405	0.89405
	y	0.0083	0.4917	0.23685	0.26315	0.5083	0.9917	0.73685	0.76315
	z	0.64455	0.14455	0.96535	0.46535	0.64455	0.14455	0.96535	0.46535

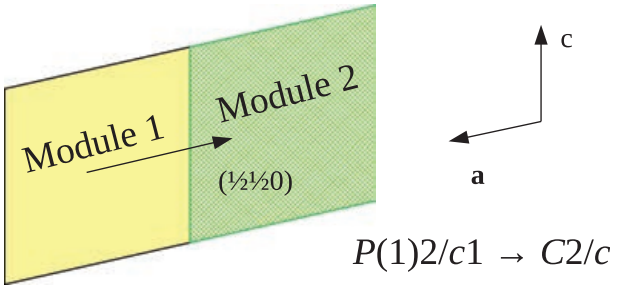

Fig. 3. Schematic view of the modular structure of clinoenstatite. The structure-building operation ($1/2\,1/2\,0$) acts on the fundamental module, of diperiodic symmetry $P(1)2/c1$ (notation after Dornberger-Schiff, 1959), leading to a triperiodic structure of symmetry $C2/c$ (Table 2). This can then be lowered to $P2_1/c$ by distortion (Table 1). (online version in colour)

4. The modular structure of protoenstatite

The structure of protoenstatite was indicated as $+-$ by Brown *et al.* (1961), *i.e.* obtained from the fundamental pyroxene module through one cell-twinning operation about a plane at the boundary of the module. The unit cell of protoenstatite has half the period along **a** with respect to that of orthoenstatite so that the metric transformation is $\mathbf{a}_{\text{proto}} = \mathbf{a}_{\text{clino}} + 1/2\mathbf{c}_{\text{clino}}$. If we apply this transformation to the low-clinoenstatite cell parameters given above, we obtain $a = 9.1281$ Å, $b = 8.8131$ Å, $c = 5.170$ Å, $\beta = 92.760°$, which are close to the cell parameters of the protoenstatite - $a = 9.306$ Å, $b = 8.886$, $c = 5.36$ Å (Yang & Ghose, 1995). The β angle deviates from 90°, which means that the cell-twinned clinoenstatite is only pseudo-orthorhombic. Besides the metric transformation, we need a shift of the origin to move the fundamental pyroxene module in a position matching half of the structure of protoenstatite. There is however no group-subgroup relation between *Pbcn* (protoenstatite) and $P2_1/c$ (clinoenstatite) compatible with the metric relation between the unit cells of the two polymorphs so that the shift of the origin to obtain a comparable description of the two models (cell-twinned clinoenstatite and protoenstatite) is not known *a priori* but can be found by moving the atoms of the clinoenstatite described in the pseudo-orthorhombic setting to the corresponding positions in the protoenstatite setting. With this constraint, the axial transformation becomes:

$$\begin{aligned} &\mathbf{a}_{\text{proto}} = \mathbf{a}_{\text{clino}} + 1/2\mathbf{c}_{\text{clino}};\ \mathbf{b}_{\text{proto}} = \mathbf{b}_{\text{clino}};\\ &\mathbf{c}_{\text{ortho}} = \mathbf{c}_{\text{clino}};\ \text{origin shift } 3/3\,1/4\,0\\ &x_{\text{proto}} = x_{\text{clino}} + 3/4;\ y_{\text{proto}} = y_{\text{clino}} + 1/4;\\ &z_{\text{ortho}} = -1/2x_{\text{clino}} + z_{\text{clino}} - 3/8 \end{aligned} \qquad (1)$$

A modular model of the protoenstatite can then be obtained by cell-twinning of the clinoenstatite through the following steps Fig. 4:

- The atomic coordinates of clinoenstatite are transformed in a pseudo-orthorhombic setting through the transformation in Eq. (1);
- the first module (+) spans half of the structure and is bounded at $x = 1/4$ and is common to clino- and protoenstatite;
- the second module (−) is obtained from the first one by a (100) *b*-glide at $x = 1/4$ in the pseudo-orthorhombic setting.

The results are shown in Tables 3–4, where for each of the two modules and for each atom in that module the closest atom in the experimental structure of protoenstatite is listed next, followed by the absolute value of the difference in the fractional coordinates (δ). With respect to the published coordinates, an alternative, equivalent description of the experimental structure is obtained by a 2-fold rotation about the [010] direction and passing through the origin (coordinates transformation: $xyz \rightarrow x\bar{y}\bar{z}$), which is one of the operations

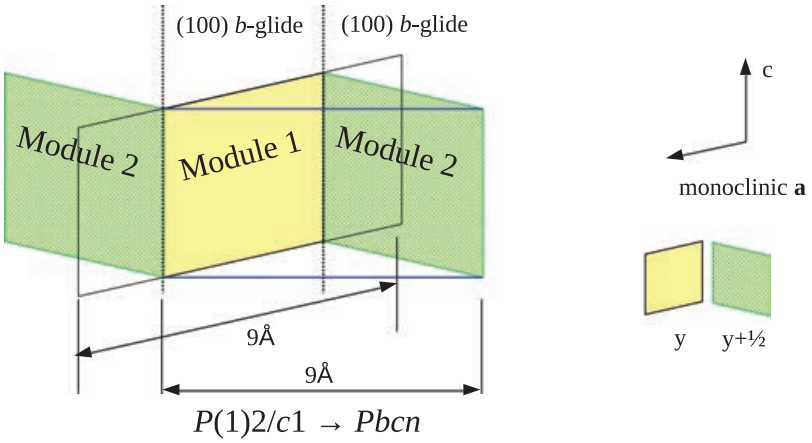

Fig. 4. Schematic view of the modular structure of protoenstatite. The structure-building operation is this time a (100) *b*-glide reflection at the boundary of the fundamental module, *i.e.* at $^1/_4yz$ in the axial setting of protoenstatite (blue unit cell). The result is a triperiodic structure of symmetry *Pbcn* (Tables 3 and 4). (online version in colour)

Table 3. Comparison of the fractional coordinates of the cell-twinned clinoenstatite and of the experimental protoenstatite structure in the *Pbcn* setting. Starting module with $-0.25 \leq x \leq 0.25$. Differences in the fractional coordinates (δ) are given as absolute values.

		Clino	Proto	δ	Clino	Proto	δ	Clino	Proto	δ	Clino	Proto	δ
Mg	*x*	0	0	0.00000	0	0	0.00000	0	0	0.00000	0	0	0.00000
	y	0.9033	0.8997	0.00360	0.0967	0.1003	0.00360	0.26312	0.2621	0.00102	0.73688	0.7379	0.00102
	z	0.75	0.75	0.00000	0.25	0.25	0.00000	0.75	0.75	0.00000	0.25	0.25	0.00000
Si	*x*	−0.20165	−0.2072	0.00555	−0.20165	−0.2072	0.00555	0.20165	0.2072	0.00555	0.20165	0.2072	0.00555
	y	0.58903	0.5901	0.00107	0.41097	0.4099	0.00107	0.58903	0.5901	0.00107	0.41097	0.4099	0.00107
	z	0.863105	0.9258	0.06270	0.363105	0.4258	0.06270	0.636895	0.5742	0.06270	0.136895	0.0742	0.06270
O	*x*	−0.12145	−0.1184	0.00305	−0.12145	−0.1184	0.00305	−0.1216	−0.1225	0.00090	−0.1216	−0.1225	0.00090
	y	0.91025	0.9053	0.00495	0.08975	0.0947	0.00495	0.7417	0.7454	0.00370	0.2583	0.2546	0.00370
	z	0.405825	0.4207	0.01488	0.905825	0.9207	0.01488	0.91625	0.9328	0.01655	0.41625	0.4328	0.01655
O	*x*	−0.14405	−0.1511	0.00705	−0.14405	−0.1511	0.00705	0.12145	0.1184	0.00305	0.12145	0.1184	0.00305
	y	0.48685	0.5153	0.02845	0.51315	0.4847	0.02845	0.08975	0.0947	0.00495	0.91025	0.9053	0.00495
	z	0.106675	0.1929	0.08623	0.606675	0.6929	0.08623	0.594175	0.5793	0.01488	0.094175	0.0793	0.01488
O	*x*	0.1216	0.1225	0.00090	0.1216	0.1225	0.00090	0.14405	0.1511	0.00705	0.14405	0.1511	0.00705
	y	0.2583	0.2546	0.00370	0.7417	0.7454	0.00370	0.51315	0.4847	0.02845	0.48685	0.5153	0.02845
	z	0.08375	0.0672	0.01655	0.58375	0.5672	0.01655	0.893325	0.8071	0.08623	0.393325	0.3071	0.08623

Table 4. Comparison of the fractional coordinates of the cell-twinned clinoenstatite and of the experimental protoenstatite structure in the *Pbcn* setting. Module with $0.25 \leq x \leq 0.75$ obtained from the starting module through a (100) *b*-glide at $x = 0.25$. Differences in the fractional coordinates (δ) are given as absolute values.

		Clino	Proto	δ	Clino	Proto	δ	Clino	Proto	δ	Clino	Proto	δ
Mg	*x*	0.5	0.5	0.00000	0.5	0.5	0.00000	0.5	0.5	0.00000	0.5	0.5	0.00000
	y	0.4033	0.3997	0.00360	0.5967	0.6003	0.00360	0.76312	0.7621	0.00102	0.23688	0.2379	0.00102
	z	0.75	0.75	0.00000	0.25	0.25	0.00000	0.75	0.75	0.00000	0.25	0.25	0.00000
Si	*x*	0.70165	0.7072	0.00555	0.70165	0.7072	0.00555	0.29835	0.2928	0.00555	0.29835	0.2928	0.00555
	y	0.08903	0.0901	0.00107	0.91097	0.9099	0.00107	0.08903	0.0901	0.00107	0.91097	0.9099	0.00107
	z	0.863105	0.9258	0.06270	0.363105	0.4258	0.06270	0.636895	0.5742	0.06270	0.136895	0.0742	0.06270
O	*x*	0.62145	0.6184	0.00305	0.62145	0.6184	0.00305	0.6216	0.6225	0.00090	0.6216	0.6225	0.00090
	y	0.41025	0.4053	0.00495	0.58975	0.5947	0.00495	0.2417	0.2454	0.00370	0.7583	0.7546	0.00370
	z	0.405825	0.4207	0.01488	0.905825	0.9207	0.01488	0.91625	0.9328	0.01655	0.41625	0.4328	0.01655
O	*x*	0.64405	0.6511	0.00705	0.64405	0.6511	0.00705	0.37855	0.3816	0.00305	0.37855	0.3816	0.00305
	y	0.98685	1.0153	0.02845	0.01315	0.0153	0.02845	0.58975	0.5947	0.00495	0.41025	0.4053	0.00495
	z	0.106675	0.1929	0.08623	0.606675	0.6929	0.08623	0.594175	0.5793	0.01488	0.094175	0.0793	0.01488
O	*x*	0.3784	0.3775	0.00090	0.3784	0.3775	0.00090	0.35595	0.3489	0.00705	0.35595	0.3489	0.00705
	y	0.7583	0.7546	0.00370	0.2417	0.2454	0.00370	0.01315	−0.0153	0.02845	0.98685	1.0153	0.02845
	z	0.08375	0.0672	0.01655	0.58375	0.5672	0.01655	0.893325	0.8071	0.08623	0.393325	0.3071	0.08623

obtained by decomposing the Euclidean normaliser of *Pbcn* with respect to the group. A simple inspection of the results shows the close similarity between the model obtained by cell-twinning of the monoclinic module and the experimental structure. The fact that Mg atoms show two sets of four equal δ values is not accidental: it is a consequence of the distribution of the Mg atoms in two orbits in *Pbcn*, each of them of multiplicity 4. Similarly, Si and O atoms show sets of eight equal δ values, as the Wyckoff positions they occupy have multiplicity eight. When taking into account the metric differences between the pseudo-orthorhombic cell of the model and the experimental orthorhombic cell, the degree of lattice distortion is 0.0117, the maximum distance of paired atoms is 0.5313 Å, the arithmetic mean is 0.2401 Å and the measure of similarity is 0.064.

5. The modular structure of orthoenstatite

The structure of orthoenstatite was indicated as ++−− by Brown *et al*. (1961); Ohashi (1984) gave the position of the glide planes transforming the clinoenstatite to orthoenstatite at $\frac{1}{4}$ and $\frac{3}{4}$ of **a** axis of the orthorhombic unit cell.

The axial transformation given by Ito, and the corresponding one from the monoclinic cell with obtuse monoclinic angle, have been reported above but the origin shift was not determined. To compare the atomic coordinates and find this origin shift it is useful to pass through an intermediate transformation via a monoclinic cell with doubled **a** parameter, which will be indicated a ''clino2'' below. The axial setting and coordinate transformations are as follows Fig. 5:

$$\begin{aligned}
&\mathbf{a}_{\text{ortho}} = 2\mathbf{a}_{\text{clino}} + \mathbf{c}_{\text{clino}};\mathbf{b}_{\text{ortho}} = \mathbf{b}_{\text{clino}};\\
&\mathbf{c}_{\text{ortho}} = \mathbf{c}_{\text{clino}};\text{origin shift } {}^1\!/_2 00\\
&x_{\text{ortho}} = {}^1\!/_2 x_{\text{clino}} - {}^1\!/_4; y_{\text{ortho}} = y_{\text{clino}};\\
&z_{\text{ortho}} = -{}^1\!/_2 x_{\text{clino}} + z_{\text{clino}} + {}^1\!/_4
\end{aligned} \tag{2a}$$

$$\begin{aligned}
&\mathbf{a}_{\text{ortho}} = \mathbf{a}_{\text{clino2}} + \mathbf{c}_{\text{clino2}};\mathbf{b}_{\text{ortho}} = \mathbf{b}_{\text{clino2}};\\
&\mathbf{c}_{\text{ortho}} = \mathbf{c}_{\text{clino2}};\text{origin shift } {}^1\!/_4 00\\
&x_{\text{ortho}} = x_{\text{clino2}} - {}^1\!/_4; y_{\text{ortho}} = y_{\text{clino2}};\\
&z_{\text{ortho}} = -{}^1\!/_2 x_{\text{clino2}} + z_{\text{clino2}} + {}^1\!/_4
\end{aligned} \tag{2b}$$

The change of the origin ($^1\!/_2$ along the **a** of the original monoclinic unit cell, or $^1\!/_4$ along the **a** of the doubled unit cell) is added for compatibility with the group-subgroup relation *Pbca* to $P2_1/c$ between ortho- and clinoenstatite.

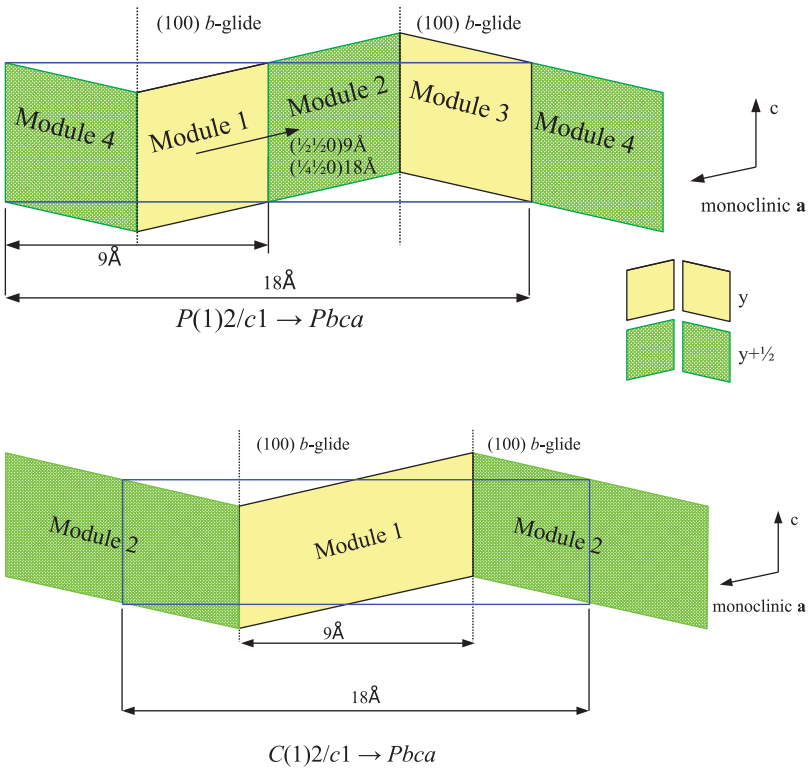

Fig. 5. Schematic view of the modular structure of orthoenstatite. (Top) Two structure-building operations act alternatively, which are the same resulting in the clino- and protoenstatite when acting separately. The translation becomes ($^1\!/_4{}^1\!/_2 0$) when expressed in the 18Å unit cell. The result is a triperiodic structure of symmetry *Pbca* (blue unit cell) (Tables 5–8). (Bottom) The same result is obtained starting from a module corresponding to a unit cell of the high-clinoenstatite (i.e. obtained by the first structure-building operation), of diperiodic symmetry $C(1)2/c1$, acting with a (100) *b*-glide reflection at $^1\!/_4 yz$ in the axial setting of orthoenstatite. This is the easiest way to find the global and partial operations by a groupoid analysis, as shown in section 7.3. (online version in colour)

Table 5. Comparison of the fractional coordinates of the cell-twinned clinoenstatite and of the experimental orthoenstatite structure in the *Pbca* setting. Starting module with $0.25 \leq x \leq 0.5$ with coordinates transformed to the pseudoorthorhombic setting according to Eq. (2b). Differences in the fractional coordinates (δ) are given as absolute values.

		Clino	Ortho	δ	Clino	Ortho	δ	Clino	Ortho	δ	Clino	Ortho	δ
Mg	*x*	0.375	0.37584	0.00084	0.375	0.37584	0.00084	0.375	0.37677	0.00177	0.375	0.37677	0.00177
	y	0.6533	0.65383	0.00053	0.8467	0.84617	0.00053	0.01312	0.01313	0.00001	0.48688	0.48687	0.00001
	z	0.875	0.866	0.00900	0.375	0.366	0.00900	0.875	0.8589	0.01610	0.375	0.3589	0.01610
Si	*x*	0.274175	0.27173	0.00244	0.274175	0.27173	0.00244	0.475825	0.47353	0.00229	0.475825	0.47353	0.00229
	y	0.33903	0.34155	0.00252	0.16097	0.15845	0.00252	0.33903	0.33739	0.00164	0.16097	0.16261	0.00164
	z	0.011895	0.0505	0.06240	0.488105	0.5505	0.06240	0.761895	0.798	0.03611	0.261895	0.298	0.03611
O	*x*	0.314275	0.31657	0.00230	0.314275	0.31657	0.00230	0.3142	0.31106	0.00314	0.3142	0.31106	0.00314
	y	0.66025	0.6602	0.00005	0.83975	0.8398	0.00005	0.4917	0.5023	0.01060	1.0083	0.9977	0.01060
	z	0.530825	0.5347	0.00387	0.030825	0.0347	0.00387	0.04125	0.0433	0.00205	0.54125	0.5433	0.00205
O	*x*	0.302975	0.30322	0.00025	0.302975	0.30322	0.00025	0.435725	0.43757	0.00185	0.435725	0.43757	0.00185
	y	0.23685	0.27738	0.04045	0.26315	0.2227	0.04045	0.83975	0.8402	0.00045	0.66025	0.6598	0.00045
	z	0.231675	0.3311	0.09943	0.731675	0.8311	0.09943	0.719175	0.6999	0.01928	0.219175	0.1999	0.01928
O	*x*	0.4358	0.43258	0.00322	0.4358	0.43258	0.00322	0.447025	0.44742	0.00040	0.447025	0.44742	0.00040
	y	0.0083	0.0173	0.00900	0.4917	0.4827	0.00900	0.26315	0.3048	0.04165	0.23685	0.1952	0.04165
	z	0.20875	0.1895	0.01925	0.70875	0.6895	0.01925	0.018325	0.1039	0.08558	0.518325	0.6039	0.08558

Such a transformation brings the atoms in the first module to coincide approximatively with one fourth of the atoms in the structure of orthoenstatite (Table 5).

A structural model for orthoenstatite can then be obtained by composing four modules in the following way:

- the first module (Table 5) is the one located between $x = 1/4$ and $x = 1/2$ in the ''clino2'' cell, with coordinates transformed in the pseudo-orthorhombic setting according to Eq. (2b);
- the second module (Table 6) is obtained by the ($1/4\,1/2\,0$) translation in the ''clino2'' cell, followed by a change of coordinates to the pseudo-orthorhombic setting according to Eq. (2b);
- the third module (Table 7) is obtained from the second one by a (100) *b*-glide at $x = 3/4$ in the pseudo-orthorhombic setting;
- the fourth module (Table 8) is obtained from the first one by a (100) *b*-glide at $x = 1/4$ in the pseudo-orthorhombic setting.

The results in Tables 5–8 compare the model and experimental structure of orthoenstatite (Ohashi, 1984) with the same presentation seen in Tables 3–4 for protoenstatite. Here again, by simple inspection the close similarity between the model obtained by cell-twinning of the monoclinic module and the experimental structure is evident. All atoms show two sets of eight equal δ values, which reflects the multiplicity of the general Wyckoff position (8*c*) in *Pbca*. When taking into account the metric differences between the pseudo-orthorhombic cell obtained by cell-twinning of clinoenstatite and the orthorhombic cell of protoenstatite, the degree of lattice distortion is 0.114, the

Table 6. Comparison of the fractional coordinates of the cell-twinned clinoenstatite and of the experimental orthoenstatite structure in the *Pbca* setting. Module with $0.5 \leq x \leq 0.75$ obtained from the starting module through ($1/4\,1/2\,0$) translation in the monoclinic cell. Resulting coordinates transformed to the pseudoorthorhombic setting according to Eq. (2b). Differences in the fractional coordinates (δ) are given as absolute values.

		Clino	Ortho	δ	Clino	Ortho	δ	Clino	Ortho	δ	Clino	Ortho	δ
Mg	*x*	0.625	0.62416	0.00084	0.625	0.62416	0.00084	0.625	0.62323	0.00177	0.625	0.62323	0.00177
	y	0.1533	0.15383	0.00053	0.3467	0.34617	0.00053	0.51312	0.51313	0.00001	0.98688	0.98687	0.00001
	z	0.625	0.634	0.00900	0.125	0.134	0.00900	0.625	0.6411	0.01610	0.125	0.1411	0.01610
Si	*x*	0.524175	0.52647	0.00229	0.524175	0.52647	0.00229	0.725825	0.72827	0.00245	0.725825	0.72827	0.00245
	y	0.83903	0.83739	0.00164	0.66097	0.66261	0.00164	0.83903	0.84155	0.00252	0.66097	0.65845	0.00252
	z	0.738105	0.702	0.03611	0.238105	0.202	0.03611	0.511895	0.4495	0.06240	1.011895	0.9495	0.06240
O	*x*	0.564275	0.56243	0.00184	0.564275	0.56243	0.00184	0.5642	0.56742	0.00322	0.5642	0.56742	0.00322
	y	0.16025	0.1598	0.00045	0.33975	0.3402	0.00045	0.9917	0.9827	0.00900	0.5083	0.5173	0.00900
	z	0.280825	0.3001	0.01928	0.780825	0.8001	0.01928	0.79125	0.8105	0.01925	0.29125	0.3105	0.01925
O	*x*	0.552975	0.55258	0.00039	0.552975	0.55258	0.00039	0.685725	0.68343	0.00229	0.685725	0.68343	0.00229
	y	0.73685	0.6952	0.04165	0.76315	0.8048	0.04165	0.33975	0.3398	0.00005	0.16025	0.1602	0.00005
	z	0.981675	0.8961	0.08558	0.481675	0.3961	0.08558	0.469175	0.4653	0.00388	0.969175	0.9653	0.00388
O	*x*	0.6858	0.68894	0.00314	0.6858	0.68894	0.00314	0.697025	0.69678	0.00024	0.697025	0.69678	0.00024
	y	0.5083	0.4977	0.01060	0.0083	0.0023	0.01060	0.76315	0.7227	0.04045	0.73685	0.7773	0.04045
	z	0.95875	0.9567	0.00205	0.45875	0.4567	0.00205	0.768325	0.6689	0.09943	0.268325	0.1689	0.09943

Table 7. Comparison of the fractional coordinates of the cell-twinned clinoenstatite and of the experimental orthoenstatite structure in the *Pbca* setting. Module with $0.75 \leq x \leq 1.0$ obtained from the previous module through a (100) *b*-glide at $x = 0.75$. Differences in the fractional coordinates (δ) are given as absolute values.

		Clino	Ortho	δ	Clino	Ortho	δ	Clino	Ortho	δ	Clino	Ortho	δ
Mg	*x*	0.875	0.87584	0.00084	0.875	0.87584	0.00084	0.875	0.87677	0.00177	0.875	0.87677	0.00177
	y	0.6533	0.65383	0.00053	0.8467	0.84617	0.00053	0.01312	0.01313	0.00001	0.48688	0.48687	0.00001
	z	0.625	0.634	0.00900	0.125	0.134	0.00900	0.625	0.6411	0.01610	0.125	0.1411	0.01610
Si	*x*	0.975825	0.97353	0.00229	0.975825	0.97353	0.00229	0.774175	0.77173	0.00245	0.774175	0.77173	0.00245
	y	0.33903	0.33739	0.00164	0.16097	0.16261	0.00164	0.33903	0.34155	0.00252	0.16097	0.15845	0.00252
	z	0.738105	0.702	0.03611	0.238105	0.202	0.03611	0.511895	0.4495	0.06240	1.011895	0.9495	0.06240
O	*x*	0.935725	0.93757	0.00185	0.935725	0.93757	0.00185	0.9358	0.93258	0.00322	0.9358	0.93258	0.00322
	y	0.66025	0.6598	0.00045	0.83975	0.8402	0.00045	0.4917	0.4827	0.00900	0.0083	0.0173	0.00900
	z	0.280825	0.3001	0.01928	0.780825	0.8001	0.01928	0.79125	0.8105	0.01925	0.29125	0.3105	0.01925
O	*x*	0.947025	0.94742	0.00040	0.947025	0.94742	0.00040	0.814275	0.81657	0.00229	0.814275	0.81657	0.00229
	y	0.23685	0.1952	0.04165	0.26315	0.3048	0.04165	0.83975	0.8398	0.00005	0.66025	0.6602	0.00005
	z	0.981675	0.8961	0.08558	0.481675	0.3961	0.08558	0.469175	0.4653	0.00388	0.969175	0.9653	0.00388
O	*x*	0.8142	0.81106	0.00314	0.8142	0.81106	0.00314	0.802975	0.80322	0.00025	0.802975	0.80322	0.00025
	y	1.0083	0.9977	0.01060	0.4917	0.5023	0.01060	0.26315	0.2227	0.04045	0.23685	0.2773	0.04045
	z	0.95875	0.9567	0.00205	0.45875	0.4567	0.00205	0.768325	0.6689	0.09943	0.268325	0.1689	0.09943

Table 8. Comparison of the fractional coordinates of the cell-twinned clinoenstatite and of the experimental orthoenstatite structure in the *Pbca* setting. Module with $0 \leq \times \leq 0.25$ obtained from the starting module through a (100) *b*-glide at $\times \in = 0.25$. Differences in the fractional coordinates (δ) are given as absolute values.

		Clino	Ortho	δ	Clino	Ortho	δ	Clino	Ortho	δ	Clino	Ortho	δ
Mg	*x*	0.125	0.12416	0.00084	0.125	0.12416	0.00084	0.125	0.12323	0.00177	0.125	0.12323	0.00177
	y	0.1533	0.15383	0.00053	0.3467	0.34617	0.00053	0.51312	0.51313	0.00001	0.98688	0.98687	0.00001
	z	0.875	0.866	0.00900	0.375	0.366	0.00900	0.875	0.8589	0.01610	0.375	0.3589	0.01610
Si	*x*	0.225825	0.22827	0.00245	0.225825	0.22827	0.00245	0.024175	0.02647	0.00229	0.024175	0.02647	0.00230
	y	0.83903	0.84155	0.00252	0.66097	0.65845	0.00252	0.83903	0.83739	0.00164	0.66097	0.66261	0.00164
	z	0.988105	0.0505	0.93761	0.488105	0.5505	0.06240	0.761895	0.798	0.03611	0.261895	0.298	0.03611
O	*x*	0.185725	0.18343	0.00230	0.185725	0.18343	0.00230	0.1858	0.18894	0.00314	0.1858	0.18894	0.00314
	y	0.16025	0.1602	0.00005	0.33975	0.3398	0.00005	0.0083	0.0023	0.01060	0.5083	0.4977	0.01060
	z	0.530825	0.5347	0.00387	0.030825	0.0347	0.00387	0.04125	0.0433	0.00205	0.54125	0.5433	0.00205
O	*x*	0.197025	0.19678	0.00024	0.197025	0.19678	0.00024	0.064275	0.06243	0.00185	0.064275	0.06243	0.00185
	y	0.73685	0.7773	0.04045	0.76315	0.7227	0.04045	0.33975	0.3402	0.00045	0.16025	0.1598	0.00045
	z	0.231675	0.3311	0.09943	0.731675	0.8311	0.09943	0.719175	0.6999	0.01928	0.219175	0.1999	0.01928
O	*x*	0.0642	0.06742	0.00322	0.0642	0.06742	0.00322	0.052975	0.05258	0.00039	0.052975	0.05258	0.00039
	y	0.5083	0.5173	0.00900	0.9917	0.9827	0.00900	0.76315	0.8048	0.04165	0.73685	0.6952	0.04165
	z	0.20875	0.1895	0.01925	0.70875	0.6895	0.01925	0.018325	0.1039	0.08558	0.518325	0.6039	0.08558

maximum distance of paired atoms is 0.5335 Å, the arithmetic mean is 0.2403 Å and the measure of similarity is 0.064. We note that despite the different stability fields of the two orthorhombic polymorphs, the degree of pseudosymmetry of the cell-twinned clinoenstatite model is practically the same.

6. The modular structure of the other pyroxenes

The structures of the four polymorphs of enstatite can be described as cell-twins of a common module. By making abstraction from the chemical differences, the same conclusions can be applied to the whole solid solutions in the enstatite-ferrosilite interval and to the other monoclinic pyroxenes, which are isostructural with either low-clinoenstatite (pigeonites) or high-clinoenstatite (augites, jadeite, spodumene).

Omphacite crystallises in two polymorphs, with space-group types *C*2/*c* at high temperature and *P*2/*n*, which is an alternative setting of *P*2/*c*, at low temperature. The phase transition from *C*/2*c* to $P2_1/c$ or to *P*2/*c* leads to splitting of the Wyckoff positions (Wondratschek, 1993), which allows chemical ordering. This is not realised in clinoenstatite, whereas the cations in the octahedral sites of omphacite undergo ordering as a result of the phase transition and each of the two sites, M1 and M2, splits in two subtypes which are then differently occupied in the low-temperature omphacite.

We make reference to the structure of a low-temperature titanian omphacite reported by Curtis *et al*. (1975), who gave cell parameters $a = 9.622$ Å, $b = 8.8825$ Å, $c = 5.279$ Å, $\beta = 106.92°$, comparable to those of clinoenstatite.

Table 9. Atomic coordinates of omphacite (structure in *P2/n*: Curtis *et al.*, 1975), idealized to the *C2/c* supergroup but still described in the subgroup (idealized structure in in the setting of *P2/n*), corresponding description in the supergroup (idealized structure in the setting of *C2/c*), and comparison with the coordinates of the idealized clinoenstatite in the same setting.

Structure in *P2/n*					Idealized structure in the setting of *P2/n*				Idealized structure in the setting of *C2/c*				Idealized clinoenstatite (see Table 1)		
Atomic site	Wyckoff position	*x*	*y*	*z*	*x*	*y*	*z*	Displacement (Å)	Wyckoff position	*x*	*y*	*z*	*x*	*y*	*z*
M1	**2***f*	0.75	0.657	0.25	0.75	0.65355	0.25	0.304	4*e*	1/2	0.90355	1/4	1/2	0.90330	1/4
M11	2*e*	0.75	0.8499	0.75	0.75	0.84645	0.75	0.304							
M2	**2***f*	0.75	0.0524	0.25	0.75	0.0497	0.25	0.0238	4*e*	1/2	0.2997	1/4	1/2	0.26312	1/4
M22	2*e*	0.75	0.453	0.75	0.75	0.4503	0.75	0.0238							
Si 1	4*g*	0.0402	0.8472	0.2298	0.03915	0.84105	0.2326	0.0579	8*f*	0.28915	0.59105	0.2326	0.29835	0.58903	0.26228
Si 2	4*g*	0.0381	0.6651	0.7354	0.03915	0.65895	0.7326	0.0579							
O 11	4*g*	0.8655	0.841	0.1223	0.86385	0.8303	0.1392	0.1339	8*f*	0.11385	0.5803	0.1392	0.12145	0.58975	0.15490
O 12	4*g*	0.8622	0.6804	0.6561	0.86385	0.6697	0.6392	0.1339							
O 21	4*g*	0.1154	0.0091	0.3095	0.10965	0.0042	0.30735	0.0686	8*f*	0.35965	0.7542	0.30735	0.37840	0.74170	0.35545
O 22	4*g*	0.1039	0.5007	0.8052	0.10965	0.4958	0.80735	0.0686							
O 31	4*g*	0.1077	0.766	0.0082	0.1023	0.7615	0.00505	0.0638	8*f*	0.3523	0.4885	0.50505	0.35595	0.48685	0.53465
O 32	4*g*	0.0969	0.743	0.5019	0.1023	0.7385	0.50505	0.0638							

Table 9 is obtained in the same way as Table 1 for clinoenstatite, *i.e.* by small displacement of atomic positions to reach the positions of the idealized structure in the *C*2/*c* supergroup. This requires ignoring the chemical difference in the M sites, which actually lead to the splitting of the Wyckoff positions and are responsible for the lower symmetry. For the ease of comparison, the last column repeats the corresponding coordinates of the idealized clinoenstatite: the close similarity is evident at a glance. From the idealized clinoenstatite model in the *C*2/*c* supergroup one gets the $P2_1/c$ structure of low-clinoenstatite by small atomic displacements, and the *P*2/*n* structure of omphacite by chemical ordering, with some small relaxation in the coordinates; the cell-twinning operation building the structural model of the two pyroxenes from the fundamental module is however the same.

7. Groupoid analysis of pyroxenes

A detailed and updated presentation of crystallographic space groupoids is beyond the scope of this article and will be presented elsewhere. Nevertheless, because the research on space groupoids in crystallography took its origin precisely with Ito's pioneer studies on pyroxenes, our presentation of the modular structure of these minerals would be incomplete without an update on this subject.

A structure composed by identical substructures requires three types of operations for its full description:

(1) *local operations*: these are the symmetry operations of the substructure and act only in the subspace spanned by the substructure;
(2) *partial operations*: these are operations mapping different substructures; a given partial operation is in general defined only for the pair of substructures to which it applies;
(3) *total* (*global*) *operations*: these are ordinary space-group operations valid in the whole space spanned by the structure.

The set of local operations forms a group, called the *kernel* of the substructure, which is necessarily a subperiodic group because the substructure does not span the whole crystal space. In the ordinary three-dimensional space, the kernel can be diperiodic (a layer group), monoperiodic (a rod group) or non-periodic (a point group). A structure composed by *n* identical substructures is characterized by *n* kernels, isomorphic to each other, differing for their orientation and/or position in space. The set of partial operations, instead, does not form a group but a set called the *hull*.

By taking one substructure as reference – let it be S_0 – its kernel will be indicated as K_0 and the hull as H_0. If h_j is one partial operation mapping S_j to S_0, the product K_0h_j is the whole set of partial operations mapping these two substructures: in fact, the composition of a partial operation with the set of the local operations of the target

substructure gives the whole set of mappings from S_j to S_0. The hull can therefore be written as the set of K_0h_j for all possible j.

By adjoining the kernel and the hull one obtains what Loewy (1927) has called *Mischgruppe*, a term which can be translated as *hybrid group* (Sadanaga, personal communication) or c*ompound group* (Brown, 1987), although it is not a group but a set of operations.

$$M_0 = K_0 \cup H_0 = K_0 \cup_j K_0h_j$$

The kernel K_j of the j-th substructure S_j is obtained by conjugating K_0 with h_j:

$$K_j = h_j^{-1}K_0h_j$$

This expression is the composition of the mapping $S_j \rightarrow S_0$ with the whole set of local operations of S_0 and with the opposite mapping $S_0 \rightarrow S_j$. If this is extended to different elements of the hull, say h_j and h_m, one gets the mapping from S_j to S_m via S_0:

$$h_m^{-1}K_0h_j\colon S_j \rightarrow S_0 \rightarrow S_m$$

Finally, the complete set of all the mappings obtained in this way gives the space groupoid D of the structure:

$$D = \cup_i M_i = \cup_{ij}h_i^{-1}K_0h_j$$

whose structure can be shown in a tabular form[3]:

$M_0 =$	K_0	$\cup$	K_0h_1	$\cup$	K_0h_{i2}	$\cup$	…	$\cup$	K_0h_p	$\cup$	…	$\cup$	K_0h_n
$M_1 =$	$h_1^{-1}K_0$		K_1	$\cup$	$h_1^{-1}K_0h_2$	$\cup$	…	$\cup$	$h_1^{-1}K_0h_p$	$\cup$	…	$\cup$	$h_1^{-1}K_0h_n$
$M_2 =$	$h_2^{-1}K_0$	$\cup$	$h_2^{-1}K_0h_1$		K_2	$\cup$	…	$\cup$	$h_2^{-1}K_0h_p$	$\cup$	…	$\cup$	$h_2^{-1}K_0h_n$
…	…	…	…	…	…	…	…	…	…	…	…	…	…
$M_n =$	$h_n^{-1}K_0$	$\cup$	$h_n^{-1}K_0h_1$	$\cup$	$h_n^{-1}K_0h_2$	$\cup$	…	$\cup$	$h_n^{-1}K_0h_p$	$\cup$	…	$\cup$	K_n

where the diagonal terms K_j are the kernels obtained by conjugation (Sadanaga, 1978; Sadanaga *et al*., 1980). The set-theoretical union of the hulls of the $n + 1$ hybrid groups constitutes the hull of the groupoid.

In the case of pyroxenes, the partial operations are translations (clinoenstatite), (100) *b*-glides (protoenstatite) or a combination of the two (orthoenstatite), producing what Ito (1950) called *echelon gliding* in the clinoenstatite, *alternate gliding* in the protoenstatite and *complex gliding* in the orthoenstatite.

The fundamental pyroxene module is obtained by taking half of the idealized clinoenstatite structure (obtained from the fractional coordinates in Table 1), for example with $0 \leq x \leq 0.5$, doubling the x fractional coordinate to simulate a fictitious structure composed by only one module. The corresponding space group is compatible with a space group of type $P2/c$. Accordingly, the kernel of the fundamental pyroxene module is $P(1)2/c1$ (notation after Dornberger-Schiff, 1959; $p2/b11$–No. 16 - in volume E of the International Tables for Crystallography: Kopský & Litvin, 2010), which is a diperiodic group because the module is a layer lacking periodicity along the **a** direction.

7.1. Groupoid analysis of clinoenstatite

The groupoid of clinoenstatite is obtained by the set-theoretical union of the hybrid groups, the hull of each being generated by a single cell-twinning operation, t(½½0), in the monoclinic setting:

$P(1)2/c1$	$P(1)2/c1\ t^{-1}(½½0)$
$t(½½0)P(1)2/c1$	$t(½½0)P(1)2/c1\ t^{-1}(½½0)$

Note that $t^{-1}(½½0)$ occurs in the first line of the groupoid, because the set of operations $P(1)2/c1\ t^{-1}(½½0)$ relates the second module to the first. Since t(½½0) gives the opposite relation and since the operations are applied from the left, the partial operation is here $t^{-1}(½½0)$. The second diagonal term is the kernel of the second module. The conjugation of $P(1)2/c1$ with t(½½0) gives back $P(1)2/c1$ with a shift of the origin by a full translation along **a** of the unit cell of clinoenstatite.

The operations of a kernel are local operation of a single module N. A subset of these operations may however also act as mappings of modules $N + j$ and $N - j$ located on both sides sides of N. In other words, these local operations of the modules become total operations of the structure. This is true at least for the identity operations of each module, which become the only identity operation of the whole structure. In the case of clinoenstatite, this happens for the whole set of operations of the kernels, which are promoted to total operations of the structure, restoring the periodicity of two modules along **a** and forming a space group of type $P2/c$.

The extra-diagonal terms represent the hull of each hybrid group building the groupoid. In the first line we find the mapping of the second layer to the first; in the second line, we find the opposite mapping, of the first layer to the second. In this special, simple case, the partial operations are identical: indeed, the inverse of a translation by half the period along a lattice direction is again a translation by half the period along the same lattice direction. As a consequence, also the partial operations are active in the whole crystal space and are thus promoted to total operations. The final result is that the whole set of the operations of the groupoid is promoted to total

operations, *i.e*. the groupoid degenerates into a group. This is just the extension of the $P2/c$ by t($\frac{1}{2}\frac{1}{2}0$), which is a *C*-centring. The result is $C2/c$, which is precisely the space-group type of clinoenstatite.

7.2. Groupoid analysis of protoenstatite

Similarly to the case of clinoenstatite, the groupoid of protoenstatite is composed of two hybrid groups, each obtained by adding to the kernel the hull generated by a single cell-twinning operation, this time a (100) *b*-glide located at $x = \frac{1}{4}$ in the orthorhombic setting (the partial operation is indicated below through its Seitz symbol: Glazer *et al*., 2014):

$P(1)2/c1$ $\quad P(1)2/c1\{m_{100}|1/2\,1/2\,0\}^{-1}$
$\{m_{100}|1/2\,1/2\,0\}P(1)2/c1$ $\quad \{m_{100}|1/2\,1/2\,0\}P(1)2/c1\{m_{100}|1/2\,1/2\,0\}^{-1}$

As in the case of clinoenstatite, conjugation of $P(1)2/c1$ with the partial operation, this time $\{m100|..0\}$, gives back $P(1)2/c1$ and the local operations of the two modules in the protoenstatite structure are again promoted to total operation, leading to $P2/c$.

As in the case of clinoenstatite, the two extra-diagonal terms give the same result, a set of four operations: *b*-glide reflection at $x = \frac{1}{4}$, *n*-glide reflection at $z = \frac{1}{4}$, twofold screw rotation at $y = \frac{1}{4}$ and $z = 0$ and another twofold screw rotation at $x = \frac{1}{4}$ and $y = \frac{1}{4}$. These, together with the kernels, give *Pbcn*, *i.e*. the space-group type of protoenstatite. Here again, the whole set of partial and local operations is promoted to total operation and the groupoid degenerates to a group.

7.3. Groupoid analysis of orthoenstatite

The structure of orthoenstatite can be described as built from the fundamental pyroxene module with three partial operations: a translation by a vector t($\frac{1}{4}\frac{1}{2}0$) (in the ''clino2'' setting), and two (100) *b*-glide reflections at $x = \frac{1}{4}$ and $x = \frac{3}{4}$. The first partial operation, t($\frac{1}{4}\frac{1}{2}0$), leads to a double module whose width is twice that of the fundamental module and coincides with the full unit cell of clinoenstatite. The structure of orthoenstatite can thus also be described as built by this double module, cell-twinned on (100), which makes the groupoid analysis simpler. The kernels of the two identical substructures are obviously $C(1)2/c1$. The groupoid is thus:

$C(1)2/c1$ $\quad C(1)2/c1\ \{m_{100}|1/2\,1/2\,0\}^{-1}$
$m_{100}|1/2\,1/2\,0\}\ C(1)2/c1$ $\quad \{m_{100}|1/2\,1/2\,0\}\ C(1)2/c1\ \{m_{\ 100}|1/2\,1/2\,0\}^{-1}$

When expressed in the axial setting of the pseudo-orthorhombic unit cell, half of the translations along the orthorhombic **a** direction are lost so that only the operations of a klassengleiche subgroup of $C(1)2/c1$ remain in the supercell. This leads to two possibilities, either $P(1)2_1/c1$ or $P(1)2/c1$, both compatible with the axial transformation $2\mathbf{a} + \mathbf{c}$,**b**,**c** but with a shift of the origin by $\frac{1}{4}\frac{1}{4}0$ for the former. However, we have adopted a description of clinoenstatite in the setting of $P2_1/c$, which also implies a shift of the origin by $\frac{1}{4}\frac{1}{4}0$ with respect to $C2/c$ (Table 1). As a consequence, the axial relation in Eq. (2b) is compatible with $P(1)2_1/c1$ so that the local operations of the modules promoted to total operations of the structure form a group of type $P2_1/c$. The extra-diagonal elements of the groupoid include each eight operations about geometric elements within the unit cell; of these four are common to the hulls of both hybrid groups (*b*-glide reflection at $x = \frac{1}{4}$, *a*-glide reflection at $z = \frac{1}{4}$, twofold screw rotation at $x = \frac{1}{4}$ and $y = 0$ and another twofold screw rotation at $y = \frac{1}{4}$ and $z = \frac{1}{4}$), which are the cell-twin operations given by Ohashi (1984) in his Table 10, while the other four are not common to both hulls, *i.e*. they are not promoted to total operations. The set-theoretical union of the intersection of the kernels and of the four total operations in the hull of the groupoid gives *Pbca*, which is precisely the space-group type of orthoenstatite.

8. Discussion

The modular interpretation of the pyroxene structure shows that, making abstraction from the chemical differences and the small deviations from the idealized coordinates, pyroxenes polymorphs can be considered as polytypes. An OD interpretation was proposed by Sedlacek *et al*. (1979) based on the choice of two kinds of layers. The choice of OD layers is in general not unique (Grell, 1984). We have shown that the structures of pyroxenes can be described as based on a single common module. The partial operations relating successive layers are cell-twin operations, *i.e*. operations that map the same module in the different positions and orientations it takes in the structure. Cell-twins have been classified as follows (Nespolo *et al*., 2004):

- *polytypes*, where the configuration at the interface is not modified;
- *chemical twins*, where the configuration at the interface is modified, subdivided in:
  - *isochemical*, without modification of the chemistry at the interface;
  - *heterochemical*, where the chemical variation observed in the final structure derives from the creation or annihilation of coordination polyhedra at the boundary between two modules

Takéuchi (1997) gathered polytypes and isochemical chemical twins into a single category called *Ito twins*, term he used to indicate what Sadanaga (1978) had called polysynthetic structures. On the basis of the nature of the partial operations, this identification does not seem justified.[4]

Partial operations can be divided in two types:

(1) ordinary space group operations, not valid everywhere in the crystal space;
(2) operations for which the order of the corresponding point group operation is not an integer multiple of the order of the corresponding screw or glide translation.

The partial operations building the structures of pyroxenes from the fundamental module are precisely of the first type. A space groupoid which contains only this type of partial operations corresponds to what Ito (1938, 1950), in his investigation of pyroxenes, has called a ''twinned space group'' and the set of partial operations is Ito's ''twinning group''. Sadanaga (1978) defined polysynthetic structures precisely in this way and identified Ito's ''twinning group'' with the set-theoretical union of the groupoid hull with the identity operation; this is correct provided that the operations in the hull are combined up to closure.

Operations of the second type above can be exemplified by the well-known *hcp* stacking of spheres. Beyond the space group operations relating the pair of hexagonal layers, partial operations do exist with unconventional translation parts, like a three-fold axis parallel to the hexagonal [001] direction but with a screw component of $^1/_2$, relating an A and a B sphere. These partial operations do not form an ordinary space group. Sadanaga (1978) called ''polytypism groupoid'' the set of partial operations, to extend Ito's scheme based on the definition of a ''twinning group''. Clearly, polytypes are a larger category including polysynthetic structures as a special case. As a consequence, either Takéuchi's Ito twins are a much larger category than the polysynthetic structures which were the object of Ito's investigation, spanning both polytypes and isochemical chemical twins, as in the classification above; or, if the term has to be used as synonym of polysynthetic structures, the taxonomy proposed by Nespolo *et al*. (2004) should be slightly modified to fit the category of polytypes.

Acknowledgements: This work has been partly realized during a stay of the first author at Kyoto University as invited Professor. The critical remarks of two anonymous reviewers are thankfully acknowledged.

Notes

1. Pyroxenes with one or two types of tetrahedral chains are termed ''high pyroxenes'' and ''low pyroxenes'', respectively, in the OD theory (Sedlacek *et al*., 1979).
2. In general, the same crystal structure has more than one equivalent description with respect to the same setting and origin of the space group. The various descriptions are related by the operations obtained by coset decomposition of the Euclidean normaliser with respect to the space group. For details, see Koch *et al*. (2005).
3. Sadanaga (1978) and Sadanaga *et al*. (1980) used the letter M to indicate the groupoid, without giving a specific label to the hybrid group. On the other hand, Sadanaga (1963) used M_i (M for *Mischgruppe*) to indicate the hybrid group of the substructure S_j and D for the groupoid. We follow this older but more complete notation.
4. Let us remind that a symmetry operation can be represented in a matrix-column form, where the matrix (linear part) corresponds to a point group operation and the column (translation part) gives the translation, including in general an intrinsic component (the screw or glide component) and a localisation component, related to the position of the symmetry element with respect to the origin of the unit cell.

References

Aroyo, M.I., Perez-Mato, J.M., Capillas, C., Kroumova, E., Ivantchev, S., Madariaga, G., Kirov, A., Wondratschek, H. (2006): Bilbao crystallographic server I: databases and crystallographic computing programs. *Z. Kristallogr.*, **221**, 15–27.

Bergerhoff, G., Berndt, M., Brandenburg, K., Degen, T. (1999): Concerning inorganic crystal structure types. *Acta Crystallogr.*, **B55**, 147–156.

Boysen, H., Frey, F., Schrader, H., Eckold, G. (1991): On the Proto to Ortho-/Clino enstatite phase transformation: single crystal X-ray and inelastic neutron investigation. *Phys. Chem. Minerals*, **17**, 629–635.

Brandt, H. (1927): Über eine Verallgemeinerung des Gruppenbegriffes. *Math. Ann.*, **96**, 360–366.

Brown, R. (1987): From groups to groupoids: a brief survey. *Bull. London Math. Soc.*, **19**, 113–134.

Brown, W.L., Morimoto, N., Smith, J.V. (1961): A structural explanation of the polymorphism and transitions in $MgSiO_3$. *J. Geol.*, **69**, 609–616.

Cameron, M. & Papike, J.J. (1981): Structural and chemical variations in pyroxenes. *Am. Mineral.*, **66**, 1–50.

Capillas, C., Tasci, E.S., de la Flor, G., Orobengoa, D., Perez-Mato, J.M., Aroyo, M.I. (2011): A new computer tool at the Bilbao crystallographic server to detect and characterize pseudosymmetry. *Z. Kristallogr.*, **226**, 186–196.

Curtis, L., Gittins, J., Kocman, V., Rucklidge, J.C., Hawthorne, F.C., Ferguson, R.B. (1975): Two crystal structure refinements of a *P*2/*n* titanian ferro-omphacite. *Can. Mineral.*, **13**, 62–67.

Dornberger-Schiff, K. (1959): On the nomenclature of the 80 plane groups in three dimensions. *Acta Crystallogr.*, **12**, 173.

Ferraris, G., Makovicky, E., Merlino, S. (2008): Crystallography of modular materials. IUCr/Oxford University Press, Oxford. 384 p.

Glazer, A.M., Aroyo, M.I., Authier, A. (2014): Seitz symbols for crystallographic symmetry operations. *Acta Crystallogr.*, **A70**, 300–302.

Grell, H. (1984): How to choose OD layers. *Acta Crystallogr.*, **A40**, 95–99.

Griffen, D. T. (1992): Silicate crystal chemistry. Oxford University Press, New York. 451 p.

Hexiong, Y., Finger, L.W., Conrad, P.G., Prewitt, C.T., Hazen, R.M. (1999): A new pyroxene structure at high pressure: Single-crystal X-ray and Raman study of the *Pbcn-P*21*cn* phase transition in protopyroxene. *Am. Mineral*, **84**, 245–256.

Hugh-Jones, D. A., Woodland, A. B., Angel, R. J. (1994): The structure of high-pressure *C*2/*c* ferrosilite and crystal chemistry of high-pressure *C*2/*c* pyroxenes. *Am. Mineral.*, **79**, 1032–1041.

Ito, T. (1935): On the Symmetry of the rhombic pyroxenes. *Z. Kristallogr.*, **90**, 151–162.

— (1938): Theory of the twinned space groups. *J. Jap. Assoc. Min. Petr. Econ. Geol.*, **20**, 201–210. (in Japanese).
— (1950): X-ray studies on polymorphism. Maruzen Co, Tokyo. 231 p.
Ito, T., Sadanaga, R. (1976): On the crystallographic space groupoids. *Proc. Japan Acad.*, **52**, 119–121.
Koch, E., Fischer, W., Müller, U. (2005): Normalizers of space group and their use in crystallography. Chapter 15 *in* ''International tables for crystallography, volume A: space-group symmetry'', Th. Hahn, ed. Fifth Edition. Dordrecht/Boston/London, Springer.
Kopský, V. & Litvin, D. B. (2010): International tables for crystallography volume E: subperiodic groups. Dordrecht/Boston/London, Wiley.
Lindsley, D.H. (1980): Phase equilibria of pyroxenes at pressures $>$ 1 atmosphere. *Rev. Miner.*, **7**, 309–339.
Loewy, A. (1927): Über abstrakt definierte Transmutationssysteme oder Mischgruppen. *J. f. Math.*, **157**, 239–254.
Makovicky, E. (1997): Modularity – different types and approaches. *in* ''Modular aspects of minerals/EMU notes in mineralogy'', Vol 1, S. Merlino, ed. Eötvös University Press, Budapest, 315–343.
Morimoto, N., Fabries, J., Ferguson, A.K., Ginzburg, I.V., Ross, M., Seifert, F.A., Zussman, J., Aoki, K., Gottardi, G. (1988): Nomenclature of pyroxenes. *Am Mineral.*, **73**, 1123–1133.
Nespolo, M., Ferraris, G., Ďurovič, S., Takéuchi, Y. (2004): Twins vs. modular crystal structures. *Z. Kristallogr.*, **219**, 773–778.
Nespolo, M., Ferraris, G., Ohashi, H. (1999): Charge distribution as a tool to investigate structural details: meaning and application to pyroxenes. *Acta Crystallogr.*, **B55**, 902–916.
Ohashi, Y. (1984): Polysynthetically-Twinned Structures of Enstatite and Wollastonite. *Phys. Chem. Minerals*, **1984**(10), 217–229.
Sadanaga, R. (1963): Extension of the theory of space groups. II. Two routes to the extension. *J. Cryst. Soc. Japan*, **5**, 10–20. (in Japanese).
— (1978): Complex structures and space groupoids. *Rec. Progr. Nat. Sci. Japan*, **3**, 143–151.
Sadanaga, R., Okamura, F.P., Takeda, H. (1969): X-Ray study of the phase transformations on enstatite. *Mineral. J.*, **6**, 110–130.
Sadanaga, R., Sawada, T., Ohsumi, K., Kamiya, K. (1980): Classification of superstructures by symmetry. *J. Jap. Assoc. Min. Petr. Econ. Geol.*, Special Issue No. **2**, 23–29.
Sedlacek, P., Zedler, A., Reinecke, K. (1979): OD interpretation of pyroxenes. *Krist. Tech.*, **14**, 1055–1062.
Shimobayashi, N. (1992): Direct observation on the formation of antiphase domain boundaries in pigeonite. *Am. Mineral.*, **77**, 107–114.
Shimobayashi, N., Miura, E., Miyake, A. (1998): Molecular dynamics simulation of high-pressure clinoenstatite. *Proc. Japan Acad.*, **B74**, 105–109.
Smyth, J.R. (1974): Experimental study on the polymorphism of Enstatite. *Am. Mineral.*, **59**, 345–352.
Takéuchi, Y. (1997): Tropochemical cell-twinning. A structure building mechanism in crystalline solids. Terra Scientific Publishing Company, Tokyo.
Tasci, E.S., de la Flor, G., Orobengoa, D., Capillas, C., Perez-Mato, J.M., Aroyo, M.I. (2012): An introduction to the tools hosted in the Bilbao crystallographic server. *EPJ WebConf.*, **22**, 00009.
Warren, B.E. & Modell, D. I. (1930): The Structure of Enstatite $MgSiO_3$. *Z. Kristallogr.*, **75**, 1–14.
Wondratschek, H. (1993): Splitting of Wyckoff positions (orbits). *Mineral. Petrol.*, **48**, 87–96.
Yang, H. & Ghose, S. (1995): High temperature single crystal X-ray diffraction studies of the ortho-proto phase transition in enstatite, $Mg_2Si_2O_6$ at 1360 K. *Phys. Chem. Minerals*, **22**, 300–310.
Yoshiasa, A., Nakatsuka, A., Okube, M., Katsura, T. (2013): Single-crystal metastable high-temperature *C*2/*c* clinoenstatite quenched rapidly from high temperature and high pressure. *Acta Crystallogr.*, **B69**, 541–546.

Received 5 June 2015
Modified version received 1 August 2015
Accepted 11 August 2015